Journal of Nuclear Materials 380 (2008) 1–7

Contents lists available at ScienceDirect

Journal of Nuclear Materials

journal homepage: www.elsevier.com/locate/jnucmat

Thermal transport properties of MgO and $Nd_2Zr_2O_7$ pyrochlore by molecular dynamics simulation

P. Shukla [a], T. Watanabe [a], J.C. Nino [a], J.S. Tulenko [b], S.R. Phillpot [a,*]

[a] Department of Materials Science and Engineering, University of Florida, Gainesville, FL 32611, United States
[b] Department of Nuclear and Radiological Engineering, University of Florida, Gainesville, FL 32611, United States

ARTICLE INFO

Article history:
Received 2 May 2008
Accepted 23 June 2008

PACS:
31.15.at
31.15.xv
65.40.−b
65.40.De
66.70.−f

ABSTRACT

Atomic level simulation methods are used to determine the thermal conductivity of magnesium oxide, MgO, and pyrochlore structured neodymium zirconate, $Nd_2Zr_2O_7$, (NDZ), two potential constituents of inert-matrix fuel systems. A simple anharmonicity analysis correctly predicts that the simulated and experimental values of the thermal conductivity of MgO should be in good agreement, as we explicitly demonstrate. Likewise, they correctly predict significantly that a large correction is needed to bring consistency between the experimental and simulated thermal conductivities for NDZ. Simulations of the thermal conductivity of fine-grained polycrystals of both materials yield estimates of the temperature dependence of the interfacial conductance and of the grain-size dependence of the thermal conductivity.

1. Introduction

Most current nuclear fuels consist mainly of UO_2; as such they pose both an environmental and proliferation threat [1]. Under neutron irradiation, ^{235}U undergoes fission, releasing energy and neutrons, while ^{238}U goes through a series of reactions, generating Pu and other radioactive materials, including Np, and Am. Due to the production of Pu from ^{238}U, the environmental and proliferation threat of spent fuel is greater than that of fresh fuel. Moreover, other by-products also pose a threat to the environment by being radioactive with very long half-lives.

These problems can possibly be abated by replacing UO_2 with an inert matrix fuel (IMF). An IMF consists of a matrix made from a conventional, non-nuclear ceramic that is transparent to neutrons, into which fissile ^{239}Pu is incorporated. The key feature of the IMF concept is that by eliminating the UO_2, plutonium breeding is also eliminated. Estimates have shown that at least 90% of the Pu will be transmuted when used as a fissile phase, thereby greatly reducing the radiotoxic waste compared to that generated by mixed oxide fuel (MOX) [2]. Candidate inert matrices for IMF systems include silicon carbide and zirconia [3]. Magnesium oxide (MgO), see Fig. 1(i), has many desirable properties as a potential IMF material, including high thermal conductivity; however, it suffers from the problem of being soluble in water, particularly at high temperatures. By contrast, pyrochlore structured materials (see Fig. 1(ii)) are insoluble in water and radiation resistant. The key obstacle to their serious consideration, however, is that their thermal conductivities are significantly lower than that of UO_2 [4–8].

Medvedev and coworkers [9] proposed an MgO–ZrO_2 cercer as a potential IMF; inspired by their results, Yates et al. [10] suggested MgO-NDZ as another potential IMF. The selection of this specific pyrochlore composition (NDZ) is based in part on insights obtained from atomic-level simulations. In particular, Sickafus et al. [11] used atomic-level simulation methods to characterize the radiation tolerance of a wide range of pyrochlores ($A_2B_2O_7$). They found that the radiation tolerance increases significantly as the B ion radius increases. By contrast, Schelling et al. [8] found that the thermal conductivity increases as the B cation radius decreases. Combining these two results with the requirement of a low cross section for the capture of neutrons, neodymium zirconate, $Nd_2Zr_2O_7$ (NDZ) is identified as a suitable candidate pyrochlore material.

This MgO-NDZ cercer system is intended to combine the desirable features of its constituents: good radiation resistance, insolubility in water, and high thermal conductivity. In their study, Yates et al. [10] found that the microstructure obtained for the same composition of MgO-NDZ cercer depends on processing methods and parameters used; moreover, these different microstructures exhibited different properties. For example, magnetic stirring produced a continuous NDZ phase with agglomerates of MgO; this microstructure exhibited a higher thermal conductivity than the cercer produced by ball milling, which was homogeneous at the microstructural level, with no agglomeration of either phase.

* Corresponding author.
E-mail address: sphil@mse.ufl.edu (S.R. Phillpot).

0022-3115/$ - see front matter © 2008 Elsevier B.V. All rights reserved.
doi:10.1016/j.jnucmat.2008.06.043

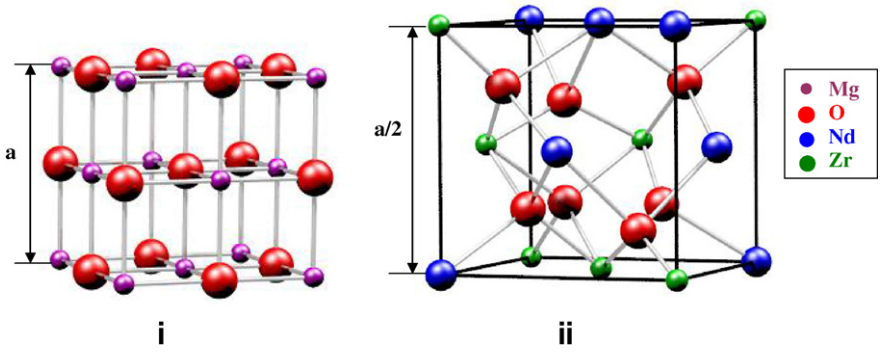

Fig. 1. Schematic of (i) unit cell of MgO, (ii) 1/8th unit cell of NDZ; the other seven octants of the unit cell can be constructed by rotations of the unit shown here (atoms are differentiated by size and colors). (For interpretation of the references to color in this figure legend, the reader is referred to the web version of this article.)

Building on the ongoing experimental studies on these cercer oxide IM compounds, here we use atomistic simulation methods to characterize the thermal transport properties of MgO and NDZ, the two constituents of the MgO-NDZ cercer. We also determine the thermal conductivity of MgO polycrystals and NDZ polycrystals with grain sizes in the sub 10 nm range, from which we estimate the grain size dependence of the thermal conductivity of larger grain size polycrystals.

2. Thermal expansion of MgO and NDZ

Molecular-dynamics (MD) simulation is the method of choice for the simulation of the thermodynamic and thermal-transport properties of electrical insulators, in which phonons are the main heat carriers. Because the long-ranged interatomic interactions in MgO and NDZ are largely ionic in nature, they can be described in MD by the Coulomb electrostatic forces. To capture the partially covalent nature of bonding in MgO and NDZ, the ions are assigned partial charges of $q_{Nd} = 2.55$, $q_{Zr} = 3.4$, $q_{Mg} = 1.7$ and $q_O = -1.7$. For computational efficiency the Coulomb energies and forces are calculated by the direct sum method [12] rather than the traditional, but slower, Ewald method.

The short-ranged repulsive interactions associated with the overlap of the valence electrons and nuclei are described by the Buckingham potential, which has the form:

$$\varphi_{ij} = A_{ij}\exp(-r_{ij}/\rho) - \frac{C_{ij}}{r_{ij}^6}, \quad (1)$$

with parameters A, ρ and C given in Table 1. The NDZ parameters are taken from Minervini et al. [13] The Mg-O parameters were determined for this study by Professor Robin Grimes, and specifically designed to be compatible with the NDZ parameters, thereby allowing the simulation of MgO-NDZ cercers, the subject of ongoing work.

The interatomic potentials are fitted to the experimental lattice parameters at room-temperature for MgO and NDZ. As a first assessment of the fidelity of these methods for the description of the thermodynamic properties of these materials, we have determined their thermal expansions. The simulation cell consists of $6 \times 6 \times 6$ cubic unit cells for MgO (a total of 1728 ions) and $4 \times 4 \times 4$ unit cells for NDZ (a total of 5632 ions), respectively. The lattice parameters of MgO and NDZ were determined as a function of temperature. As can be seen from Figs. 2 and 3, the lattice parameters predicted by the simulation are in quite good agreement with the experimental values [6,14]. As another measure of materials fidelity, we can compare the linear thermal expansion coefficients, α, extracted from these data, for the temperature range $T = 300$–1500 K. For MgO the simulated thermal expansion coefficient of $12.4 \times 10^{-6}\,K^{-1}$ is 95% of the experimental value of $13.1 \times 10^{-6}\,K^{-1}$ [15]. The agreement for NDZ is less good with the simulated value of the thermal expansion ($7.3 \times 10^{-6}\,K^{-1}$) being only 77% of the experimental value of $9.5 \times 10^{-6}\,K^{-1}$ [6]. Such levels of agreement are typical of empirical potentials for oxide materials [8,16,17].

Table 1
Buckingham potential parameters for MgO and NDZ

Species	A (eV)	ρ (Å)	C (eV Å^6)	Reference
$O^{1.7-}$–$O^{1.7-}$	35686.18	0.201	32.0	
$Nd^{2.55+}$–$O^{1.7-}$	2148.14	0.3227	22.59	[13]
$Mg^{1.7+}$–$O^{1.7-}$	929.69	0.29909	0.0	
$Zr^{3.4+}$–$O^{1.7-}$	1402.57	0.3312	5.1	[13]

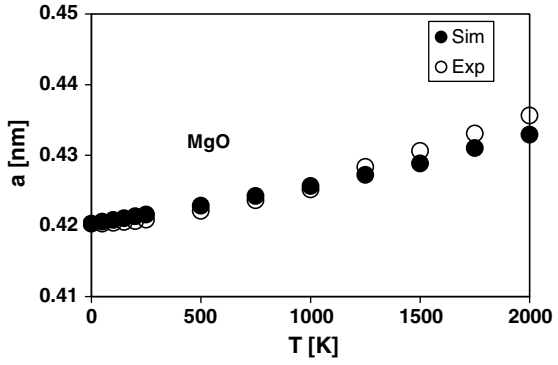

Fig. 2. Temperature dependence of the lattice parameter of MgO from simulation (solid circle) and experiment (open circle) [14].

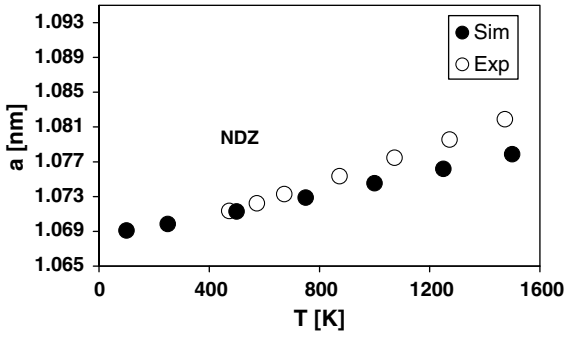

Fig. 3. Temperature dependence of the lattice parameter of NDZ from simulation (solid circle) and experiment (open circle) [6].

These differences between the simulated and experimental values provide valuable information on the nature of the interatomic interactions. As is well known, the thermal expansion arises from the asymmetry in the interaction potential, i.e., from the anharmonicity in the interatomic interactions. An elementary analysis gives the Grüneisen relation for the thermal expansion:

$$\alpha = \gamma c_v / 3B, \tag{2}$$

where c_v is the specific heat, B is the bulk modulus and γ is the Grüneisen parameter, which is a measure of the anharmonicity of the material [18]. We thus attribute the reduced values of the simulated thermal expansions to the interatomic interactions being insufficiently anharmonic and/or the bulk modulus being too high.

This conclusion has important implications for the thermal transport properties, because the thermal conductivity is also determined by the anharmonicity of the interactions. In particular, in most electrically-insulating materials the dominant scattering mechanism is phonon–phonon scattering. Such scattering would be completely absent if all of the interactions were harmonic. Using a perturbation expansion of the interatomic potential to third order, thereby including the lowest anharmonic terms, Liebfried and Schloemann showed that the thermal conductivity is inversely proportional to the square of the Grüneisen parameter [19]:

$$\kappa \sim \frac{24}{10}\frac{\sqrt{4}}{\gamma^2}\left(\frac{k_B}{h}\right)^3 Mv\frac{\theta^3}{T}, \tag{3}$$

where k_B is the Boltzmann constant, h is the Planck constant, v and M are the volume and the mass per atom. The only two materials constants that enter into Eq. (3) are the Debye temperature, θ, and the frequency-averaged Grüneisen parameter, γ. From this relation, it is clear that the thermal conductivity decreases with increasing anharmonicity.

Through their dependence on the Grüneisen parameter, we can derive a simple empirical relationship between the thermal conductivity and thermal expansion [20]:

$$\alpha^2\kappa = \chi\frac{\theta^3 C_v^2}{B}. \tag{4}$$

The constant χ contains all of the non-materials constants in Eqs. (2) and (3). Table 2 shows that the values of θ and C_p for these potentials for these systems determined using GULP (General Utility lattice Program) [21,22] are very similar to the experimental values. Moreover, the experimental and calculated values of $G = \Theta^3 C_p^2$, analogous to the combination in Eq. (3) are within 20% in for both materials. We may therefore merge C_v and Θ_D with other constants in the equation. Eq. (4) then becomes

$$\kappa = \frac{\chi'}{\alpha^2 B}, \tag{5}$$

where $\chi' = \chi\theta^3 C_v^2$.

From Eq. (5), we thus predict:

$$\kappa_{sim} = \kappa_{expt}(\alpha_{expt}/\alpha_{sim})^2(B_{expt}/B_{sim}). \tag{6}$$

We have determined the bulk moduli for MgO and NDZ from simulation for these potentials to be 170 GPa and 167 GPa, respectively, at 0 K The corresponding experimental room-temperature values for single crystals are 155 GPa and 159 GPa, which are quite consistent [23,24].

From these data, Eq. (6) predicts $\kappa_{sim} = 1.02\,\kappa_{expt}$ for MgO and $\kappa_{sim} = 1.61\,\kappa_{expt}$ for NDZ; that is, our simulations of the thermal conductivity of MgO should match the experimental results rather well, while the simulations should significantly overestimate the thermal conductivity of NDZ. As we shall see in the next section, this simple analysis provides a systematic method for improving the quantitative accuracy of our thermal-conductivity simulations.

Table 2
Comparison of Debye and C_p calculated with GULP with experiment

Material	θ (K)		C_p (J/mol K)		Γ
	Sim.	Exp.	Sim.	Exp.	
MgO	830	946	38.77	34.82	0.83
$Nd_2Zr_2O_7$	549	489	207.54	232.70	1.13

$\Gamma = G_{sim}/G_{expt}$, where $G = \Theta_D^3 C_p^2$, analogous to the term in Eq. (4).

3. Thermal conductivity of MgO and NDZ

Fourier's Law states that a heat flux, J, through a material results in a temperature gradient, dT/dx. The proportionality constant between the two is the thermal conductivity, κ:

$$J = -\kappa\frac{dT}{dx}. \tag{7}$$

The two most commonly applied methods for computing thermal conductivity within MD simulations are the 'direct method' [25,26] and the 'Green–Kubo method' [27–29]. The direct method is a non-equilibrium method in which a heat current is passed through the simulation cell, resulting in a temperature gradient, see Fig. 4; it is thus a direct implementation of Fourier's Law. In the Green–Kubo approach the thermal conductivity is determined from autocorrelations in the heat current of a system in thermodynamic equilibrium. Direct comparisons on the two methods have previously been shown to yield identical results within the statistical errors [12]. Because of its ease of implementation, and its applicability for polycrystalline materials, we use the direct method in this study.

For the simulations of single crystals, the simulation cell is a long thin square cylinder with edges parallel to the ⟨001⟩ crystallographic directions. The narrow directions form the x–y (001) plane; the long direction is along the z [001] axis and is parallel to thermal gradient. The simulation cell is 4×4 unit cells in the x–y plane, which previous studies indicate is sufficient to obtain size-independent results [12]. The key determinant of the thermal conductivity is the mean free path of the phonons before they scatter from each other or components of the microstructure. If the system-size in the direction of heat flow is smaller than the phonon mean free path, then the intrinsic anharmonic properties of the system will not be probed completely. This regime is known as the Casimir limit. It is thus no surprise that previous studies have also shown that the thermal conductivity depends significantly on the length of the simulation cell. In a previous study, we have identified a finite size scaling approach that allows the intrinsic thermal conductivity of the material to be determined [12]. This approach, which is based on the inverse additivity of contributions to the mean free path, yields:

$$\frac{1}{\kappa} = \frac{1}{\kappa_\infty} + \frac{4P}{L_z}, \tag{8}$$

where κ is the thermal conductivity determined from simulation, κ_∞ is the thermal conductivity in the infinite system-size limit (i.e., our best estimate of the 'true' thermal conductivity of the material), L_z is the length of the simulation cell and P is a constant. Eq. (8) thus suggests that a plot of $1/\kappa$ vs. $1/L_z$ should be linear, and that the thermal conductivity of an infinite system can be obtained by extrapolating to $1/L_z = 0$. Fig. 5 shows such analysis for MgO and NDZ at 573 K. We indeed find the expected linear dependences. By using above described system size analysis at various temperatures, we have extracted the temperature dependence of the thermal conductivity for both MgO and NDZ.

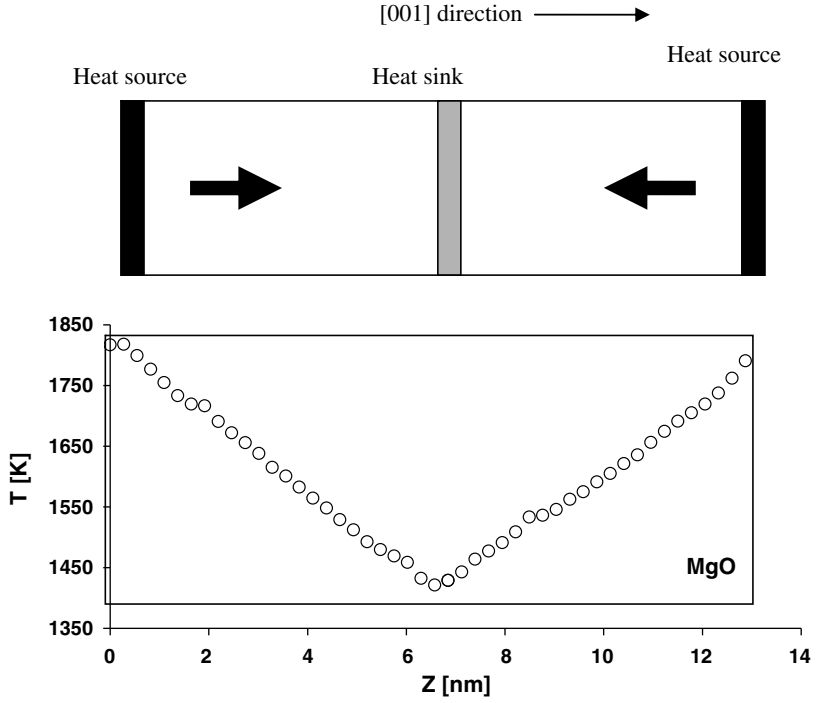

Fig. 4. Schematic of the simulation cell, showing the heat source, heat sink and directions of heat flow, and a typical temperature profile from which the thermal conductivity is extracted using Fourier's Law.

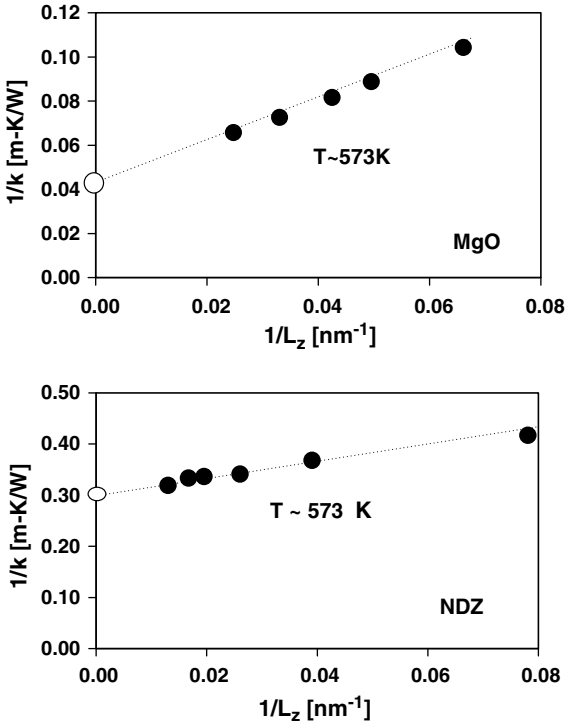

Fig. 5. κ_∞ calculation using system size analysis for MgO and NDZ at 573 K.

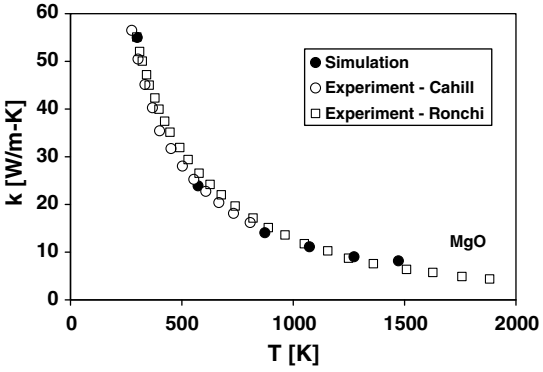

Fig. 6. Thermal conductivity data of MgO: experiment data for single crystal thin film (open circle) [30], experiment polycrystal data (open square [31]) and simulation data (solid circle).

Finite-size scaling analysis can lead to a significant increase in the simulated value of thermal conductivity, as is illustrated in Fig. 5. If only a single simulation had been performed for the shortest simulation cell (L_z = 15.3 nm for MgO and L_z = 12.80 nm for NDZ), then the estimated thermal conductivities would be less than one-fourth of the best estimated value.

Fig. 6 compares the best estimate of the thermal conductivity determined from simulation and finite-size scaling analysis, with the experimental data for MgO. The data of Cahill (open circles) [30] is for a high-quality single crystal thin film, while the polycrystalline data (solid triangles) is for coarse-grained polycrystal [31]. The experimental polycrystalline data is systematically lower than the experimental data for a single crystal by a small amount. While physically this is reasonable since the polycrystals contain grain boundaries, and possibly other defects arising from processing, all of which provide additional scattering mechanisms, this difference could also be simply statistical in origin [32]. The simulated data (solid circles) agree very well with the single crystal experimental data. Had a finite size analysis not been performed, these values would have been significantly lower and would not have agreed with the experimental values. That the experimental and simulated values are in such good agreement provides validation for the harmonic analysis described in the previous section, which predicted that they should agree within 2%.

The anharmonicity analysis performed in the previous section yielded a multiplicative correction factor of 1/1.61 = 0.62 to be applied to the value of the NDZ thermal conductivity determined

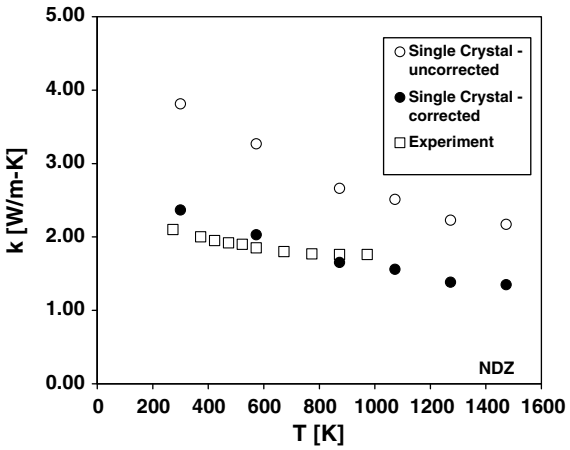

Fig. 7. Thermal conductivity of NDZ: uncorrected single crystal simulation values (open circle), corrected single crystal values (solid circle) and experimental polycrystal values (open square) [5].

directly from the simulation. Fig. 7 shows both the uncorrected and corrected predictions for the thermal conductivity of NDZ. While the uncorrected values are, as we expect, consistently higher than the experimental values, the corrected values are much more consistent with the experimental results.

Thus, the combination of careful simulations, systematic analysis of the effects of the finite size of the simulation cell, and the analysis of the anharmonicity in the system leads to calculated values of the thermal conductivity that are in quantitative or semi-quantitative agreement with the experimental results.

4. Thermal conductivity of polycrystalline MgO and NDZ

The simulations described above were performed on perfect single crystals. However, few materials are single crystals; none are completely defect free. To characterize the effects of grain boundaries, we have determined the thermal conductivity of model polycrystals of MgO and NDZ. To amplify the interface effect to the highest degree, we simulate polycrystals with extremely small grain sizes, in this case only ~3 nm. It is possible to extend this size range into the tens of nanometers range but, due to intrinsic computational limitations, it is not possible to extend the range to the microns and tens of microns grain size, present in typical ceramic materials.

Fig. 8 shows the simple model polycrystal used for this study. This polycrystal is textured with all of the grains being oriented parallel to the [001] axis in the *z*-direction (normal to the figure). For both MgO and NDZ, each of the 24 perfectly hexagonal grains are filled with perfect crystal with the [100] directions oriented in almost random orientations with respect to the horizontal *x*-axis, with the stipulation that all grain-boundary misorientations should be >15°, thereby reducing the tendency for grain coalescence. The grain boundaries in these polycrystals are thus a reasonably random selection of ⟨001⟩ tilt boundaries. Periodic boundary conditions are applied such that there are no additional interfaces at the boundaries. The final steps in the generation of the polycrystal are to ensure overall charge neutrality, and to remove the few ions in the grain boundaries that are too close to each other.

The thermal conductivity is calculated by the same approach as was used for single crystals: a heat current is imposed on the system, which results in a temperature gradient. The effect of system size is expected to be much less important for such fine-grained polycrystals because the dominant mechanism should be phonon/grain boundary rather than phonon/phonon scattering; indeed, simulations on the system shown in Fig. 8 and a system with the same microstructure and grain size, but twice the length (formed by simply putting two simulation cell shown in Fig. 8 end to end), gave thermal conductivity values within 5% of each other, which is within the statistical errors of the simulations.

We recall that the anharmonicity analysis predicted the thermal conductivities of the single crystals from simulations would be overestimates by 2% for MgO, but 62% for NDZ. In predicting the thermal conductivity of the polycrystalline materials below, we apply these same anharmonic corrections. In this step, we have assumed that the thermal expansion and bulk modulus are essentially microstructure independent. We are aware that this is not strictly true. However, within the approximation made in separating the contributions in the polycrystal thermal conductivity from that of grain interior and gain boundary, the accuracy may not be sufficient to consider more detailed analysis.

As Figs. 9 and 10 show, the calculated thermal conductivities of the fine-grained polycrystals of MgO and NDZ are considerably smaller than their single-crystal counterparts. The thermal conductivity for polycrystalline NDZ shows a smaller reduction from the single-crystal value than does polycrystalline MgO (note the difference in scales); we attribute this smaller reduction to the already much smaller mean free path of phonons in NDZ as compared to MgO. Also, for both systems, the effect is considerably larger at lower temperatures, at which the phonon mean free path is longer.

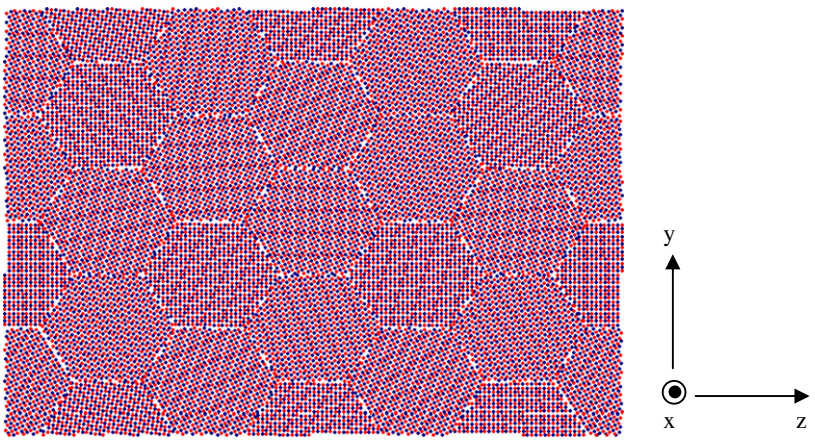

Fig. 8. One atomic plane in the textured polycrystalline microstructure of MgO used in these simulations. The grain size is ~3 nm.

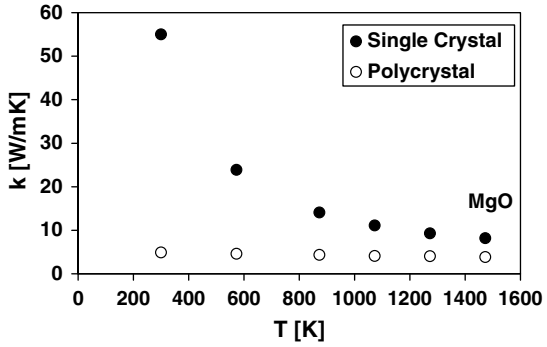

Fig. 9. Comparison of thermal conductivity of MgO: single crystal (solid circle) and 3 nm polycrystal (open circle).

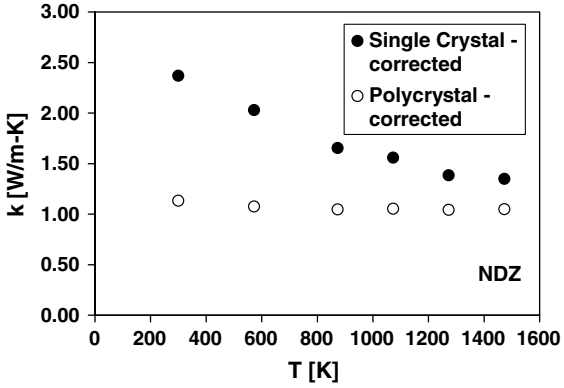

Fig. 10. Comparison of corrected thermal conductivity of NDZ: single crystal (solid circle) and 3 nm polycrystal (open circle).

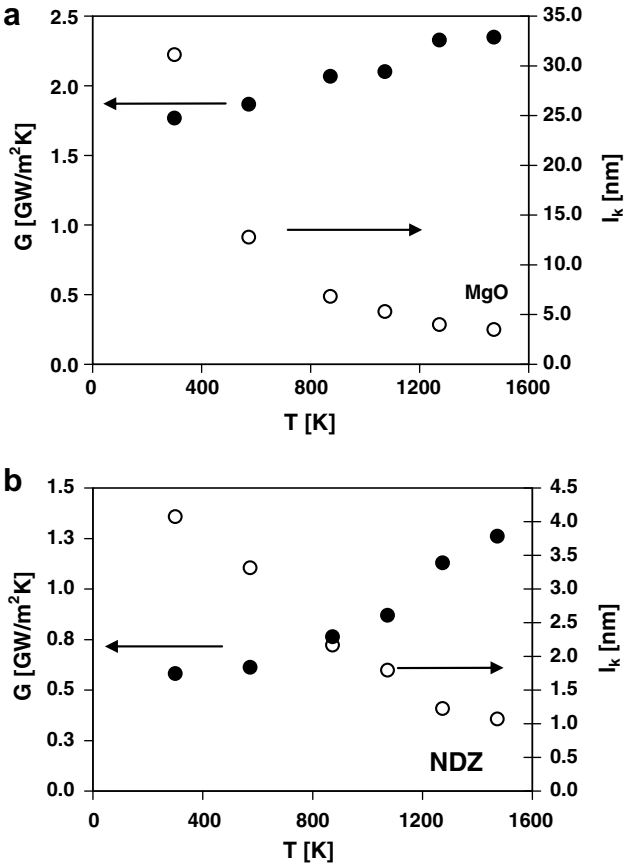

Fig. 11. Temperature dependence of the interfacial conductance, G (solid symbols) and Kapitza length, l_k (open circles) for (a) 3 nm polycrystalline MgO and (b) 3 nm polycrystalline NDZ.

Using a simple model in which the polycrystal is assumed to be describable in terms of a volume of bulk with thermal conductivity (κ_0) and a volume of grain boundary with interface conductance (G) (all grain boundaries being assumed to be physically the same), Yang et al. [33] derived a simple relation for the dependence of the thermal conductivity, κ of a polycrystal on grain size, d:

$$\kappa = \kappa_0/(1 + \kappa_0/Gd). \tag{9}$$

Using Eq. (9), we have extracted estimates for G; the result is shown in Fig. 11 for both, MgO and NDZ. As for other materials that have been studied experimentally and/or in simulation, G increases with temperature, reflecting the enhanced anharmonic coupling of weakly coupled phonon modes across the interfaces [34].

Because the thermal conductivity and G are in different units, it is not possible to compare them directly. To make a comparison possible, l_k is defined as κ_0/G and it is a measure of the length of perfect crystal that offers the same resistance to heat transport as the interface, i.e., the larger the value of l_k, the larger the thermal barrier offered by the interface. The temperature dependence of the Kapitza length l_k for MgO and NDZ are shown in Fig. 11. For MgO, $l_k \sim 30$ nm at 300 K which decreases to $\sim$3 nm at 1473 K. The effect is less dramatic in NDZ, with l_k decreasing from 4 nm at 300 K to 1.75 nm at 1473 K. These decreases are consistent with the trends seen previously for UO_2 [20] and diamond [35], in both of which, the temperature dependence of l_k decreased with temperature for both materials.

Having determined G, Eq. (9) can now be used to predict the grain-size dependence of the thermal conductivity. Fig. 12 shows the calculated grain size dependence of the thermal conductivity at 300 K and 573 K for MgO and NDZ, normalized to the corresponding single crystal values; thus in both cases, the large grain

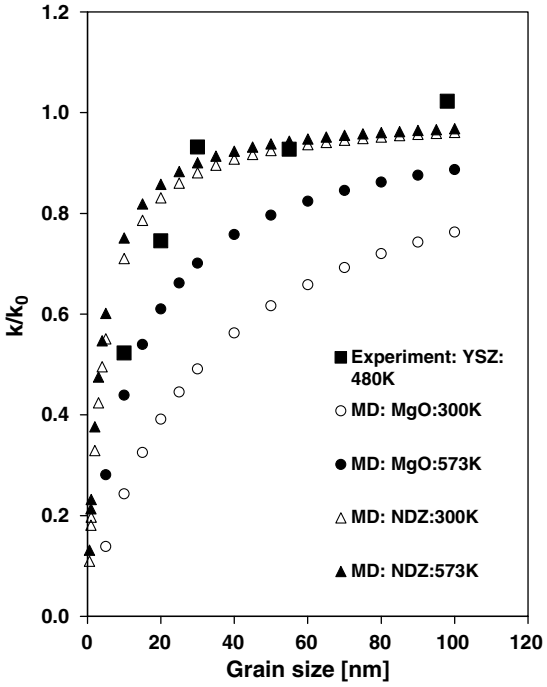

Fig. 12. Predicted grain size dependence of the normalized thermal conductivity of MgO (solid and open circle) and NDZ (solid and open triangle) polycrystals compared with experimental results of YSZ (solid square) [33].

size limit is $\kappa/\kappa_0 = 1$. In the absence of any experimental data on the thermal conductivity of MgO or NDZ as a function of grain size against which to compare these trends, Fig. 12 includes the experimental results of Yang et al. [33] for yttria-stabilized zirconia (YSZ). Despite the considerable difference in materials and microstructures (textured vs. random polycrystal), the simulation data is broadly consistent with the experimental data. In particular, the agreement between the simulation results for NDZ and the experiments for YSZ is remarkably good; this agreement probably arises from the fact that they are both low thermal conductivity materials with fluorite-related crystal structures.

5. Discussion

Experimental values for the bulk modulus and thermal expansions of ceramic materials are much more widely available than are thermal conductivity data. The results of this study and our previous study on UO_2 [20] show that the fidelity of a potential for quantitatively predicting the thermal conductivity of a material can be estimated from a comparison of the simulated thermal expansion coefficient and bulk modulus with experimental values. Indeed, these results indicate the importance of using the bulk modulus and thermal expansion coefficient as key fitting parameters for new potentials. While the elastic properties, including the bulk modulus, have long been included in fitting data for ionic potentials, the thermal expansion typically has not. The thermal expansion has traditionally been omitted from the fitting set because it is a finite temperature property. While such finite temperature properties are typically determined by time-consuming MD simulations, they can also be determined with some precision (particularly at low temperatures) in the quasi-harmonic approximation. Indeed, this capability is available in the widely used General Utility Lattice Program (GULP) [21,22]. The opportunity thus exists for the development of potentials for oxides with significantly improved thermal-transport properties. This simple analysis of the thermal expansion and thermal conductivity based on the Grüneisen relation points to a simple approach for predicting the error in the calculated thermal conductivity. This will be of particular value for systems in which experimental thermal conductivity data are not available.

The simulated thermal expansion for MgO was in excellent agreement with the experiment. With the correction determined from the anharmonicity analysis, the agreement between experiment and simulation for NDZ was good; however the simulated thermal conductivity does show a stronger temperature dependence than the experimental values.

The thermal conductivity of MgO and NDZ polycrystals (3 nm) were also investigated. Using these results, the grain size dependence on thermal conductivity was also analyzed for both the materials MgO and NDZ. The result from this analysis suggests that significant degradation of the thermal transport properties in these materials will only be evident for sub-micron grain sizes. Moreover, the good agreement between the trends in the simulated data and experimental trends in YSZ indicates that even the very oversimplified model microstructure used in these simulations captures the essential of the thermal-transport properties.

Acknowledgments

We gratefully acknowledge Professor Robin Grimes of Imperial College London for generating the interatomic potential for MgO, and for valuable discussions. We are happy to acknowledge the University of Florida High-Performance Computing Center for providing computational resources and support that have contributed significantly to the research results reported in this paper. This work was funded by DOE-NERI Award DE-FC07-05ID14647.

References

[1] R.C. Ewing, W.J. Weber, J. Lian, J. Appl. Phys. 95 (2004) 5949.
[2] K.E. Sickafus, R.J. Hanrahan, K.J. McClellan, J.N. Mitchell, C.J. Wetteland, D.P. Butt, P. Chodak, K.B. Ramsey, T.H. Blair, K. Chidester, H. Matzke, K. Yasuda, R.A. Verrall, N. Yu, Am. Ceram. Soc. Bull. 78 (1999) 69.
[3] H. Matzke, V.V. Rondinella, T. Wiss, J. Nucl. Mater. 274 (1999) 47.
[4] J.K. Fink, J. Nucl. Mater. 279 (2000) 1.
[5] J. Wu, X. Wei, N.P. Padture, P.G. Klemens, M. Gell, E. Garcia, P. Miranzo, M.I. Osendi, J. Am. Ceram. Soc. 85 (2002) 3031.
[6] H. Lehmann, D. Pitzer, G. Pracht, R. Vassen, D. Stover, J. Am. Ceram. Soc. 86 (2003) 1338.
[7] S. Lutique, R.J.M. Konings, V.V. Rondinella, J. Somers, T. Wiss, J. Alloys Compd. 352 (2003) 1.
[8] P.K. Schelling, S.R. Phillpot, R.W. Grimes, Philos. Mag. Lett. 84 (2004) 127.
[9] P.G. Medvedev, S.M. Frank, T.P. O'Holleran, M.K. Meyer, J. Nucl. Mater. 342 (2005) 48.
[10] S.J. Yates, P. Xu, J. Wang, J.S. Tulenko, J.C. Nino, J. Nucl. Mater. 362 (2007) 336.
[11] K.E. Sickafus, L. Minervini, R.W. Grimes, J.A. Valdez, M. Ishimaru, F. Li, K.J. McClellan, T. Hartmann, Science 289 (2000) 748.
[12] P.K. Schelling, S.R. Phillpot, P. Keblinski, Phys. Rev. B 65 (2002) 144306.
[13] L. Minervini, R.W. Grimes, Y. Tabira, R.L. Withers, K.E. Sickafus, Philos. Mag. A 82 (2002) 123.
[14] L.S. Dubrovinsky, S.K. Saxena, Phys. Chem. Miner. 24 (1997) 547.
[15] M.W. Barsoum, Fundamentals of Ceramics, 2nd Ed., Taylor & Francis, 2003.
[16] C.B. Basak, Comput. Mater. Sci. 40 (2007) 562.
[17] A. Senyshyn, L. Vasylechko, M. Knapp, U. Bismayer, M. Berkowski, A. Matkovskii, J. Alloy Compd. 382 (2004) 84.
[18] N.W. Ashcroft, N.D. Mermin, in: Solid State Physics, Saunders College Publishing, 1976, p. 488.
[19] G. Leibfried, E. Schloemann, Nachr. Akad. Wiss. Goettingen, Math. Physik. Kl. II a 4 (1954) 71.
[20] T. Watanabe, S.B. Sinnott, J.S. Tulenko, R.W. Grimes, P.K. Schelling, S.R. Phillpot, J. Nucl. Mater. 375 (2008) 388.
[21] J.D. Gale, J. Chem. Soc. Faraday Trans. 93 (1997) 629.
[22] J.D. Gale, A.L. Rohl, Mol. Simulat. 29 (2003) 291.
[23] D.H. Chung, Philos. Mag. 8 (1963) 833.
[24] M.P. Vandijk, K.J. Devries, A.J. Burggraaf, Solid State Ionics 9&10 (1983) 913.
[25] P. Jund, R. Jullien, Phys. Rev. B 59 (1999) 13707.
[26] R.H.H. Poetzsch, H. Bottger, Phys. Rev. B 50 (1994) 15757.
[27] J.W. Che, T. Cagin, W.Q. Deng, W.A. Goddard, J. Chem. Phys. 113 (2000) 6888.
[28] J. Li, L. Porter, S. Yip, J. Nucl. Mater. 255 (1998) 139.
[29] S.G. Volz, G. Chen, Phys. Rev. B 61 (2000) 2651.
[30] D.G. Cahill, S.M. Lee, T.I. Selinder, J. Appl. Phys. 83 (1998) 5783.
[31] C. Ronchi, J.P. Ottaviani, C. Degueldre, R. Calabrese, J. Nucl. Mater. 320 (2003) 54.
[32] P.G. Klemens, Solid State Physics 7 (1958) 45.
[33] H.S. Yang, G.R. Bai, L.J. Thompson, J.A. Eastman, Acta Mater. 50 (2002) 2309.
[34] D.G. Cahill, W.K. Ford, K.E. Goodson, G.D. Mahan, A. Majumdar, H.J. Maris, R. Merlin, S.R. Phillpot, J. Appl. Phys. 93 (2003) 793.
[35] M.A. Angadi, T. Watanabe, A. Bodapati, X.C. Xiao, O. Auciello, J.A. Carlisle, J.A. Eastman, P. Keblinski, P.K. Schelling, S.R. Phillpot, J. Appl. Phys. 99 (2006) 114301.